MICROBOONE-NOTE-1016-PUB

Noise Characterization and Filtering in the MicroBooNE TPC

The MicroBooNE Collaboration

(Dated: July 5, 2016)

In large liquid argon time projection chambers (LArTPCs), TPC signal processing, which recovers the number of ionized electrons arriving at the anode plane from the raw digitized wire signals, is a crucial step towards automated event reconstruction. The first stage of signal processing is the identification and removal of any excess TPC noise with minimal impact on the true signal.

In this technote, we characterize various TPC noise observed in the raw digital signal data in MicroBooNE and the software filtering techniques used to remove them. Although some of the sources of the excess TPC noise has not yet been conclusively identified, the noise can be efficiently removed with the software filter with minimal distortions of the TPC signal. Some efforts towards eliminating the noises with hardware upgrade are also described.

The resulting equivalent noise charge (ENC), after the software noise filter is applied, varies with wire length and is found to be around 400 electrons. The residual noise is consistent with the cold electronics design expectations and test-stand measurements.

1. INTRODUCTION

Liquid Argon Time Projection Chamber (LArTPC) [1–4] is an active 3-D tracking calorimeter that enables the detection of accelerator neutrinos and other rare events such as proton decay and burst supernova neutrinos on a large scale with unprecedented imaging capabilities. The MicroBooNE detector [5, 6] is the most recently built LArTPC designed to observe interactions of neutrinos from the on-axis Booster and off-axis NuMI beams at the Fermi National Accelerator Laboratory in Batavia, IL. The detector consists of a 2.56 m × 2.3 m × 10.4 m TPC including an array of 32 PMTs [7] that detect scintillation light and are used for triggering, timing and other purposes. The inner TPC is housed in an evacuable and foam insulated cryostat vessel. It has a 2.56 m drift length and 3 readout anode wire planes - U, V and Y in order of plane closest to the cathode - spaced 3 mm apart with 3 mm wire spacing for a total of 8,256 signal channels. The V plane is at ground while the U and Y plane are at -110 V and +230 V respectively. The active mass of the detector is 86 ton of LAr. The ionization electrons produced by an energetic charged particle track drift through the LAr to the detector wire planes along the electric field lines. Bipolar signals are induced on the wires of the U and V induction planes and a unipolar signal is produced on the Y (also called W) collection plane as illustrated in Fig. 1.

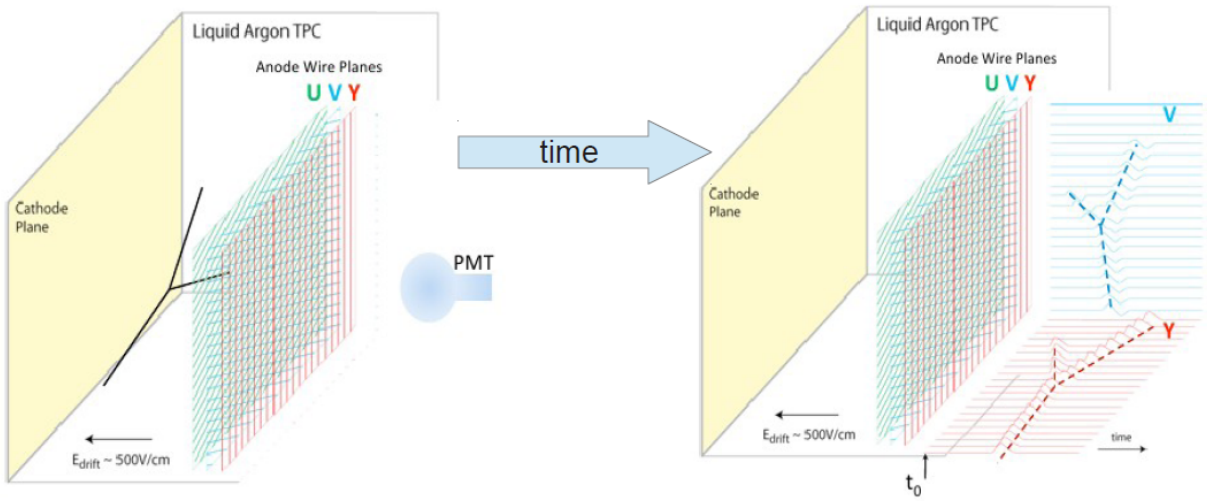

FIG. 1. Diagram illustrating the signal formation in a LArTPC with 3 wire planes.

The schematic of the MicroBooNE readout electronics is shown in Fig. 2.

The signals on the wires are amplified and shaped by the CMOS analog front-end cold readout chips (Application Specific Integrated Circuits - ASICs) [8] which are mounted on the Front End Mother Boards (FEMBs) and immersed in LAr. The analog signal from the cold electronics (CE) is then transmitted over 2–5m of twisted pair copper cable, through the warm flange, to the intermediate amplifier line driver in an enclosure forming a Faraday cage with the cryostat. From the intermediate amplifier the signal is transmitted to the TPC readout board where it is digitized by a 12-bit ADC with a 2 MHz effective sampling rate for a 4.8 ms readout duration.

The front-end ASICs are mounted on the FEMBs and placed close to the end of the readout wires, embedded inside LAr in order to minimize the capacitance and electronic noise from the amplifier. The cold ASIC can operate at four gain settings (4.7, 7.8, 14, and 25 mV/fC), which is the peak height of the shaping function, and four shaping time settings (0.5, 1.0, 2.0, 3.0 μs), which is the distance between the peak position and 5% of peak position of the shaping function. The output signals of the ASICs are sent through the intermediate amplifier, which further provides a gain of 1.1, and then digitized by a 2 MHz, 12-bit ADC (0–4096) with a dynamic range of 2 V. Each DAQ readout window is 4.8 ms in duration which corresponds to 9600 recorded samples (also called time ticks or ticks).

MicroBooNE started production data taking in October of 2015. While the cathode is designed to operate at 128 kV which corresponds to a drift electric field of 500 V/cm, MicroBooNE is currently operating with a cathode HV of only 70 kV which corresponds to a drift field of 273 V/cm. With a drift field of 273 V/cm, the ionization electrons are drifting at a speed of ∼1.114 mm/μs [9, 10]. The cold ASICs are nominally operated at 14 mV/fC gain and 2 μs shaping time. During the detector operation, the TPC noise [11] observed in the data significantly exceeded the expected noise performance of the cold electronics. In the following sections,

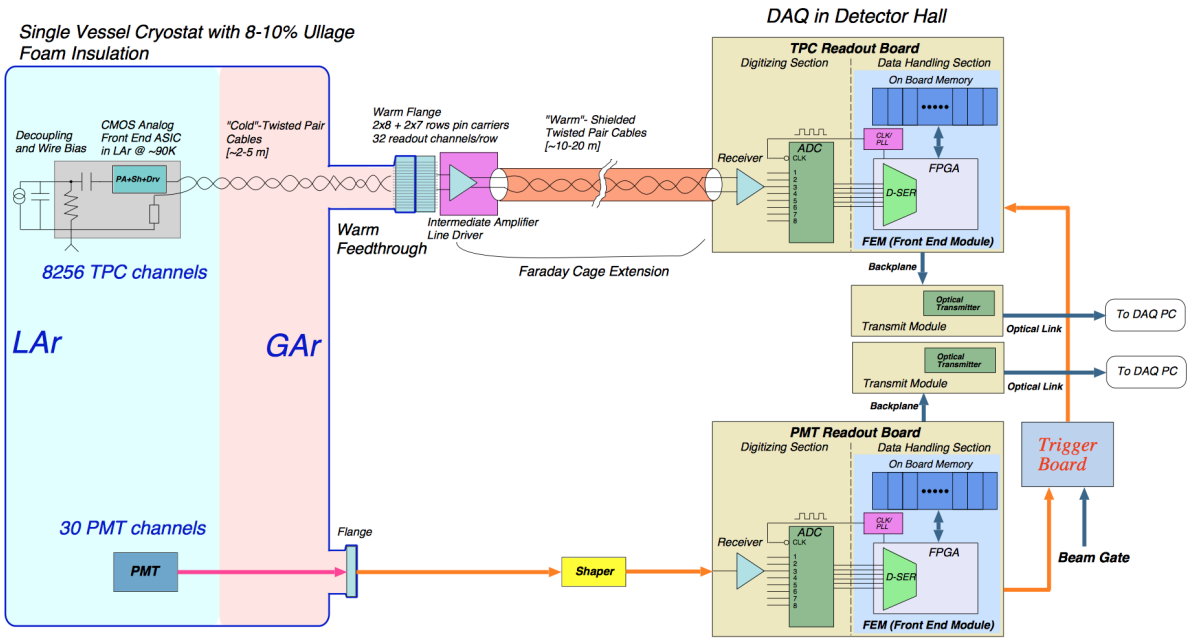

FIG. 2. Schematic of MicroBooNE cold and warm electronics readout chain [6].

we will describe the characteristics of the TPC noise observed and introduce the software filters designed to minimize the impact of the excess noise on the extraction of the ionization signals.

1.1. Cold Electronics Impulse Response and RC Filters Response

To understand and identify excess noise sources encountered in MicroBooNE LArTPC, it is necessary to define the overall impulse response of the readout from the sense wire to the input of the ADC and determine the inherent noise of the ASIC. The first step is to calibrate the charge sensitivity of the readout using a pulser and calibration capacitances in the ASIC. Excess noise sources can be analyzed by studying the sampled noise waveforms in both time and frequency domain, as well as studying their dependence on the operating conditions of the TPC (wire bias, cathode voltage) and location (wire plane, feedthrough and wire location, etc).

The cold electronics readout chain is designed as a 5th order low pass network to obtain an impulse response close to a gaussian. The impulse response function is derived from the inverse Laplace transformation [12] of the transfer function of this network. The transfer function $T(s)$ as a function of a complex number s is given in Eq. (1)

$$T(s) = \frac{A_o \cdot cA_o}{(p_0 + s) \cdot (ip_1^2 + (rp_1 + s)^2) \cdot (ip_2^2 + (rp_2 + s)^2)} \tag{1}$$

The parameters of the transfer function given in Eq. (1) are defined in Eq. (2):

$$
\begin{aligned}
p_0 &= \frac{1.477}{T_o \cdot cT_o}; \\
rp_1 &= \frac{1.417}{T_o \cdot cT_o}; \\
ip_1 &= \frac{0.598}{T_o \cdot cT_o}; \\
rp_2 &= \frac{1.204}{T_o \cdot cT_o}; \\
ip_2 &= \frac{1.299}{T_o \cdot cT_o}; \\
cA_o &= \frac{2.7433}{(T_o \cdot cT_o)^4}; \\
cT_o &= \frac{1}{1.996};
\end{aligned}
\tag{2}
$$

where the A_o is the gain parameter and T_o is the shaping time, respectively.

The impulse response function in the time domain obtained from the inverse Laplace transformation of $T(s)$ is shown in Fig. 3 (left) in terms of signal amplitude vs. time. The MicroBooNE front-end cold electronics are designed to be programmable with 4 different gain settings (4.7, 7.8, 14, and 25 mV/fC) and 4 shaping (peaking) time settings (0.5, 1, 2, and 3 μs). The gain setting is the peak height of the shaping function while the shaping time is defined as the time between peak and 5% of the peak and the time of the peak. For a fixed gain setting, the peak is always at the same height independent of the shaping time.

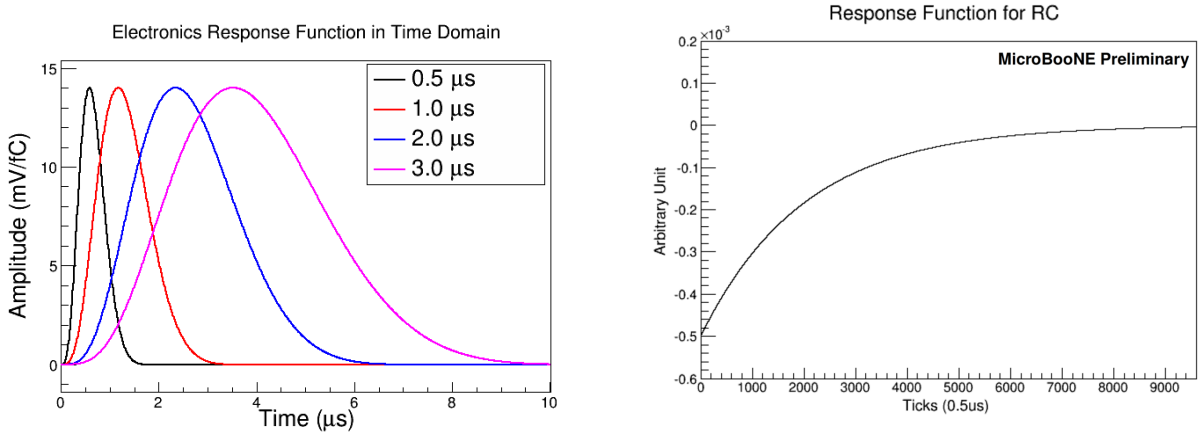

FIG. 3. ASIC's impulse response functions are shown for four shaping time settings at 14 mV/fC gain (left). Simulated response function of the RC+RC shaping in MicroBooNE. Each time tick corresponds to 0.5 μs. The initial δ function is omitted (right).

There are two RC hardware filters [13] implemented in MicroBooNE warm electronics readout system [6]. One is placed at the intermediate amplifier and the other is located at the ADC. The time constant for both circuits is 1 ms. Hence the resulting electronic response is a convolution of two RC response functions. Each RC shaping function is parameterized as $\delta(t) - e^{-t/t_0}/t_0$ with $t_0 = 1$ ms. These RC circuits introduce long tails to the impulse response and thus need to be corrected. Since the time constant is generally long (1 ms) with respect to the length of the signal, the effect is negligible when the signal is small. However, in the case of large signals (for e.g. a vertical traveling cosmic muon's signal on the vertically oriented collection wires), the effect of the RC shaping leads to a distortion of the baseline by introducing a long negative tail. Fig. 3 (right) shows the simulated overall RC shaping function, which is used to correct the signal through a deconvolution procedure [14]. Left and right panel of Fig. 4 show the signal before and after correcting for the RC shaping effect.

Although such a correction is effective in removing the distortion of the baseline, there are certain scenarios where such a correction would fail. For example, if the signal from a vertical cosmic muon arrived just before the 4.8 ms data window, the recorded data would miss the large positive primary signal, and only include the

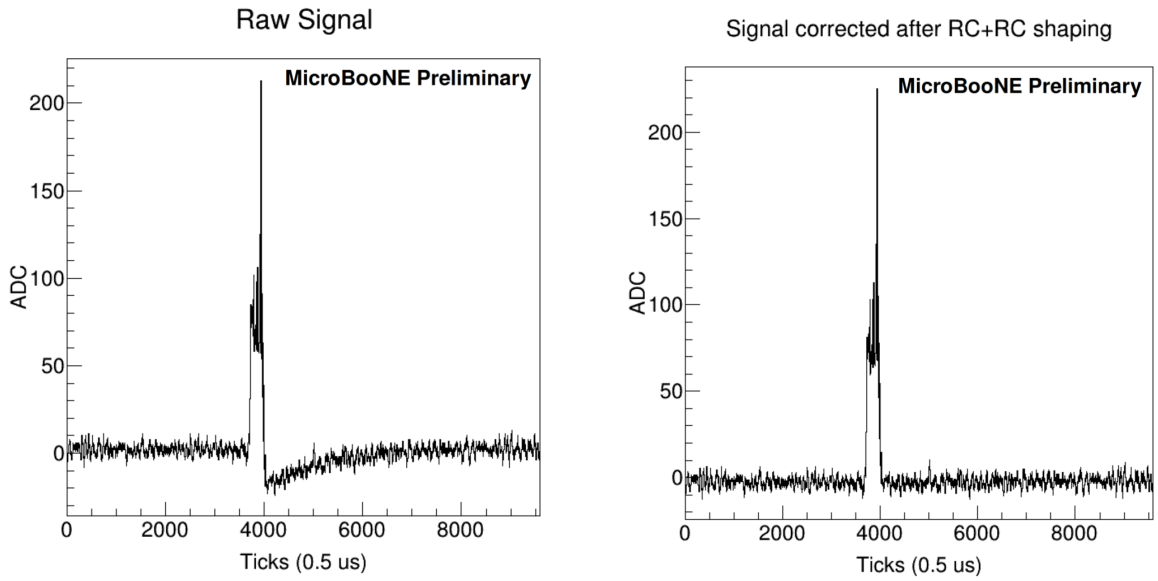

FIG. 4. Example Y-plane raw signal waveform from data Run 3455 (left) and signal after correcting for RC shaping effect. (right)

long negative tail. Applying the default deconvolution procedure on such a signal would lead to a significant baseline distortion due to short data record. Instead, these signals are identified by looking at the frequency content of the raw signal using a Fast Fourier Transform (FFT) and looking for large amplitudes at very low frequency. In this case instead if applying RC+RC correction, the baseline of these signals in time domain is corrected.

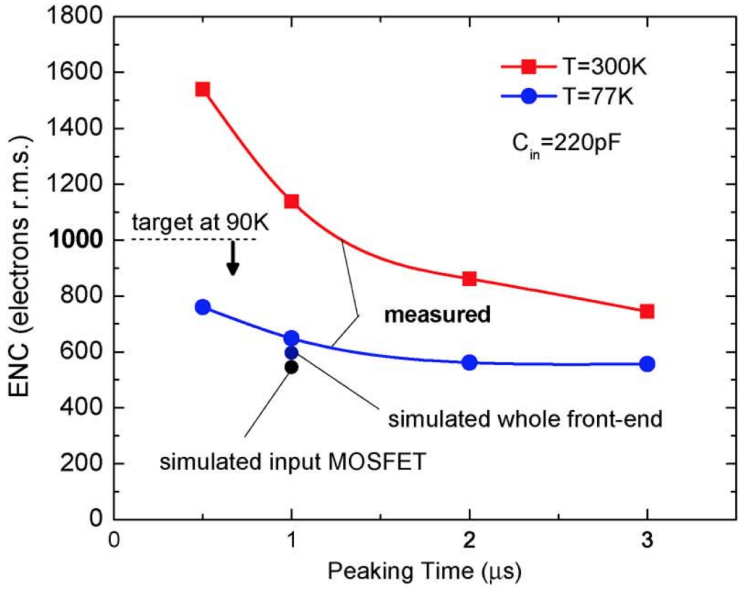

FIG. 5. Measured ENC for the analog ASIC at 300 K and 77 K at the four peaking times. The simulated ENC from the input MOSFET and from the whole analog chain is also shown [16]. The ASIC noise at 77K is dominated by the $1/f$ noise from the first transistor, for peaking times $> 1\mu$s.

2. IDENTIFICATION AND FILTERING OF MICROBOONE TPC NOISE

The TPC noise observed in MicroBooNE could come from a variety of sources, only the first one on the list below being unavoidable:

- **The noise associated with amplification in the first transistor of the cold electronic ASIC**: usually characterized by the Equivalent Noise Charge (ENC).

  By definition, ENC is "An impulse Qs δ(t) of current producing an output equal to the rms noise, such that Qs = ENC [units of charge], usually expressed in the number of electron charges, or rms electrons." Or in other words, ENC is the noise charge which produces an output of the same magnitude as an impulse signal of equal charge.

  The Equivalent Noise Charge due to the first transistor noise can be expressed as [8, 15]

$$\mathrm{ENC}^2 = \mathrm{e_n}^2 \mathrm{C_{in}}^2 / \mathrm{t_p} \tag{3}$$

  Where:
  $\mathrm{e_n}^2 = 4\mathrm{k_B T R_{sn}}$ = transistor series white noise spectral density in [V/Hz$^{1/2}$];
  $\mathrm{R_{sn}}$ = transistor equivalent series noise resistance;
  $\mathrm{C_{in}} = \mathrm{C_{wire}} + \mathrm{C_{cable}} + \mathrm{C_{ampl}}$;
  $\mathrm{t_p}$ = weighting function peaking time $\simeq$ 1/bandwidth;
  $\mathrm{k_B}$ = Boltzmann constant

  In Fig. 5, the measured and simulated ENC for the different ASIC peaking times is shown [16] for an input capacitive load of 220 pF. The capacitive load per channel of a LArTPC varies with wire length and TPC geometry, with the capacitance per m of wire length given by Eq. 4:

$$\text{Wire capacitance} = \frac{2\pi\epsilon_o\epsilon_r}{(\pi G/W) - ln(\pi d/W)} \tag{4}$$

  where ϵ_0 is the dielectric constant for air, ϵ_r is the dielectric constant for LAr, W is the wire spacing, G is the plane gap and d is the wire diameter. In MicroBooNE with a 3 mm wire spacing and a 3 mm plane gap this corresponds to 18 pF/m. The lengths of the wires in the MicroBooNE TPC vary from a few cm to 4.7 m. This noise is irreducible.

- **Electronic noise from the warm shaping amplifier and ADC:** One of the principal objectives of low noise front end design is that the readout system noise should be limited only by the noise of the first transistor. The noise of the first transistor is determined by measurements and simulations (see Ref [16]). The shaping amplifier noise is small compared to the first transistor noise. Overall ASIC noise is optimized against power dissipation [16]. The noise contributions from the intermediate amplifier and ADC are negligible (The ASIC gain should be selected so as to make the ADC quantization noise negligible).

- **Electronic noise from other circuits in the readout chain:** An example would be the low frequency coherent noise from the low voltage regulators supplying the ASIC operating voltages. This noise was expected and a filter circuit was added to the voltage regulator on the board to prevent such noise. As discussed in Sec. 2.6, a low frequency coherent noise component has been observed that is confirmed to originate from the voltage regulators. The noise filter circuit on the board is being upgraded.

- **Noise introduced by the wire bias power supplies:** This noise was carefully determined to be negligible in MicroBooNE.

- **Noise from the cathode HV:** The anode is highly sensitive to voltage fluctuations in the cathode potential, such as from the ripple from the HV supply.

- **ASIC saturation due to wire microphonics (wire motion)**: that is charge generated due to the motion of the TPC sense wires in the electric field. As described briefly in Sec. 2.4, a periodic saturation of the ASICs has been observed in MicroBooNE that may be caused by the wire motion, possibly due to the convective motion of the liquid.

Identification of different types of noise is obtained by using a combination of methods: examination of waveforms of sense wire signals recorded in the time domain, Fast Fourier Transform (FFT) of these waveforms and the equivalent noise charge (ENC) as a function of the shaping time. The FFT can identify fixed continuous wave (cw) frequency sources of noise such as that described in Sec. 2.6. FFT alone, particularly if used without phase information does not provide sufficient information. Identification of possible microphonics noise that caused the front-end ASIC to saturate (Sec. 2.4) required more complicated analysis. Finally, through examination of the ADC pedestal RMS on all channels after filtering fixed frequency noise signals, channels with very large unidentified residual noise and channels with very low noise can be characterized. For each noise signal identified a software filter is implemented to remove the noise. The different noise signals are presented below in the same sequence in which they are implemented in the software noise filter.

The noise sources identified in Sec. 2.3 and 2.6 can be removed by hardware filters with no impact on the signal. The software filter is therefore an interim measure that demonstrates the effect of removing these sources of noise. Unlike a hardware filter, this cannot be done without some impact on the signal.

2.1. Identifying Mis-Configured Channels

The expected electronics noise characteristics are different for different shaping times. The MicroBooNE TPC has a total of 8256 channels across three planes. The first 2400 channels are on the first induction (U) plane, the next 2400 are on the second induction (V) plane and remaining 3256 channels are on the collection (W or Y) plane. All these channels are grouped into 516 ASICs [5] (16 channels per ASIC). The settings selected for the production data taking have been 14 mV/fC gain and 2 μs shaping time for the production data taking. Using pulser signal analysis, it was found that 14 ASICs i.e, 224 channels, do not have the correct configurations and were stuck at lower values of gain (4.7 or 7.8 mV/fC instead of 14 mV/fC) and shaping time (1 μs instead of 2 μs). All of these channels are on the first induction plane (U-plane). We can identify these mis-configured channels with different settings by looking at the frequency content of the raw waveform obtained from the FFT, 1μs will be flatter. As shown in Fig. 6, the frequency content of the 2 μs shaping time setting signal (left panel) is clearly different from that of 1 μs (right panel).

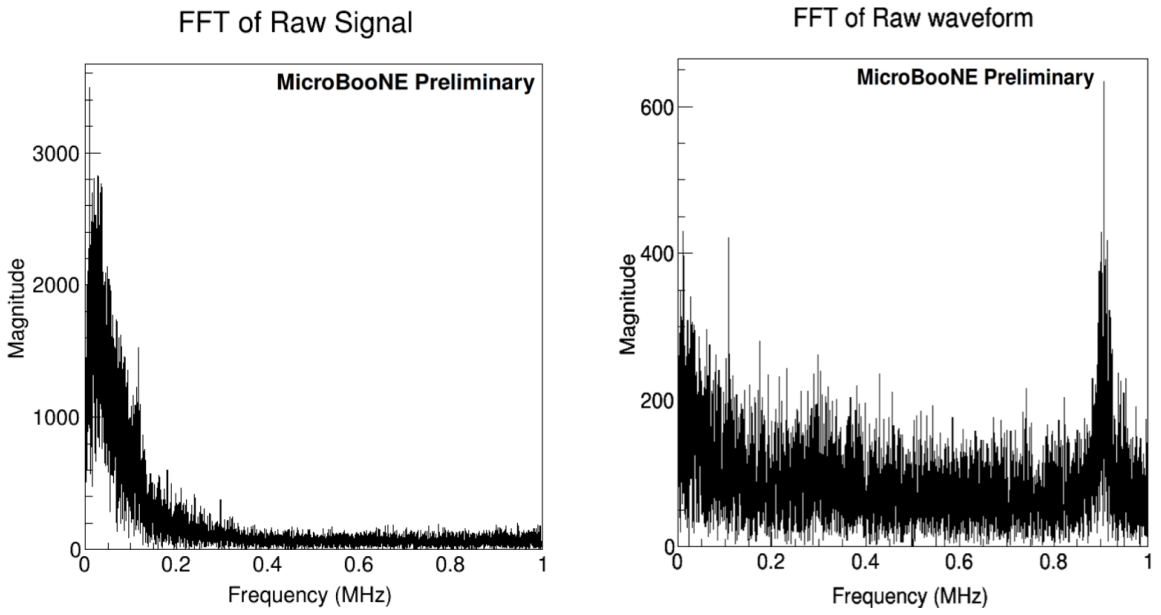

FIG. 6. The raw signal waveform of the default 2 μs shaping time (left) and that for the mis-configured 1 μs shaping time (right). Both waveforms are from the first event of Run 3455 and corresponds to a U-Plane channel. The peak around 900 kHz in the 1 μs shaping time waveform is due to the high frequency noise discussed in Sec. 2.2

Although these channels are mis-configured, they are useful as the real signals can still be seen clearly apart from the electronic noise. In treating these channels, we correct their configurations by deconvolving the incorrect response function and then convolving the correct response function (shown in Fig. 3 (left)) in software through the frequency domain.

2.2. 900 kHz Noise (Burst Noise)

Using the FFT technique, one of the first striking large fixed frequency noise signals identified shortly after MicroBooNE turn on was a high frequency noise centered around 900 kHz [17]. This noise is found on sense wires in all three anode planes, to a different degree, and is believed to be originating from field pick-up on the sense wires, as the noisy wires concentrate at one corner of the detector. This high frequency noise can be easily identified in the frequency domain. The peak in the Fig. 6 (right) around 900 kHz is due to this very high frequency noise. As expected this noise is prominent in the case of channels with lower shaping times like 0.5 μs or 1 μs, but for the default shaping time of 2 μs this noise is almost absent.

While the FFT (the frequency domain) would indicate a continuous wave at ∼900 kHz. The waveforms in the time domain indicate periodic bursts of noise, where the ringing has a period of 1.1μs corresponding to ∼900 kHz. The bursts of this noise are intermittent (non-stationary) with the amplitude varying in time. The source has not been identified. This type of noise is usually caused by power switching circuits (none of which are inside the cryostat). The fraction of events affected by this noise is small.

This high frequency noise can be completely removed by applying a low-pass frequency filter in software (which sets frequencies >730 kHz to zero) on the deconvoluted signals in the data. Given that the noise is negligible with a 2μs shaping time, there is no need to filter out the very high frequency components in the current production running [18].

2.3. The HV Power Supply Noise

Examination of noise on U-plane channels in both the time and frequency domain reveals a series of single frequency noise sources that seem to be odd harmonics of 36 kHz, the fundamental frequency of the HV power supply ripple. The two main (highest and second highest) single frequency noise components corresponds to 36 kHz and 108 kHz. There are other single frequency components also, but their amplitudes are much lower than the 36 and 108 kHz noise and therefore have minimal impact on the signal.

Considering the high drift voltage of the TPC, the ripple of the HV power supply is very small, less than 1 part in 10^5. It comes somewhat as a surprise to see how sensitive the anode plane is to tiny potential variations at the cathode 2.5 meters away. It takes only a few millivolts on the cathode to induce the current waveforms observed.

A simple estimate of this sensitivity can be made. The induced charge on the anode wire plane by cathode potential variations is calculated as follows:

- The single sense wire capacitance to cathode (2.5 m drift, 3 mm wire spacing) is ∼40 fF/m.
- Assuming a 2.5 m wire length, the induced charge would be ∼0.1 fC/mV, resulting in ∼600 e^-/mV. The expected peak amplitude of the waveform is ∼ 15 ADC counts. With the calibration of ∼200 e/ADC counts, it corresponds to ∼0.5 fC. Thus only about 5 mV at the cathode can produce the observed noise, or about 5 parts in 10^8 of the drift voltage. Thus a large attenuation by filtering is required, which not easy to realize with high voltage components.

This noise can be more easily identified than some other excess noise sources by the amplitude distribution among the wire planes, U, V and Y and dependence on HV. The noise on the V plane is attenuated due to shielding by the U-wires, and the noise on Y wire is further attenuated by shielding by the V-wires. The amplitude is fairly uniform and proportional to the wire length. The waveforms should be coherent.

In the software filter, the harmonic noise is directly removed from the frequency domain of the signal after Fourier transformation. The hardware filter solution currently under way by the HV and electronics teams, is to add an additional stage of low pass filtering between the HV supply and the cathode (an additional "beanpot").

Fig. 7 shows the effect of noise filters on the single-frequency noise components. The left panel shows an example raw digitized waveform from U-plane where it is difficult to differentiate the signal from the electronic noise. The middle panel is the same waveform after filtering out the 36 kHz noise and the right panel is after filtering out both the 36 kHz and 108 kHz noise. Two peaks from signals can be clearly identified after the noise filtration.

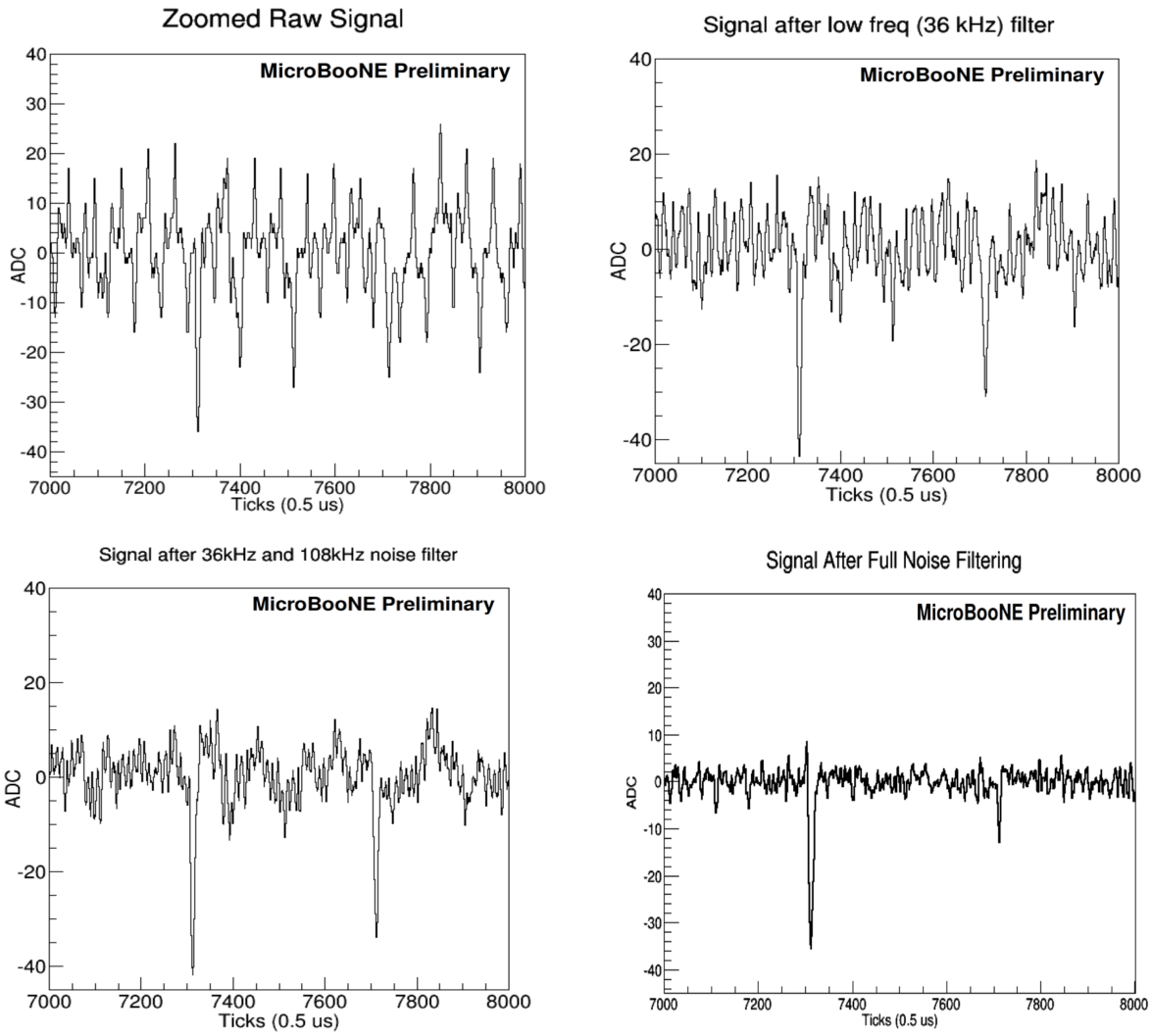

FIG. 7. A digitized U-plane raw waveform (Channel 1513) from data Run 3455 (top left), the same waveform after filtering out 36 kHz noise (top right), and the same waveform after filtering out both 36 kHz and 108 kHz noise components (bottom left) are shown. The waveform after full noise filtering chain (bottom right). 36 and 108 kHz noise is due to the HV supply ripple, and that this noise is about ∼3 times lower on the V-plane and negligible on the Y-plane

2.4. Saturation of ASICs

During the detector commissioning period, it was observed that the expected readout from some ASICs would suddenly disappear - with the channel noise RMS becoming very small - and then reappear after being off for a while. This pattern keeps repeating with periods of the ASIC channel being live for a while and recording normal signals and then reverting to a no-signal state.

At the beginning of the live period, there is usually a period of time when the baseline is distorted presumably due to the RC circuits that were described in Sec. 1.1. This kind of behavior [19] was later identified as the result of a periodic saturation of the ASICs. The input stage in the ASIC requires a bias current to maintain the preamplifier in a linear operating region. This current must be as low as possible as it contributes shot noise directly into the input. During the initial MicroBooNE run, the ASIC bias current [20] was set to 100 pA and it was observed that large fraction of channels on the induction planes (10-15%) and a few on the collection plane would experience periodic saturation. After resetting the ASIC bias current to 500 pA, the incidence of saturation was greatly reduced. The remaining periodic saturation of the ASICs

is time dependent and the total number of channels affected is around 300 channels per event [21]. The accurate determination of the frequency of the periodic saturation from the data is difficult due to the data records being short compared to the saturation period (4.8 ms vs 100 ms) Direct scope measurements at the output of the intermediate amplifier of several U and V channels that periodically saturate indicates that the saturation effect has very low frequencies of < 15 Hz, but could have different frequencies on different wires.

In order to deal with this kind of behavior, the region corresponding to the saturation needs to be identified on an event-by-event basis and labeled as a dead region for the later stages of the analysis chain. Furthermore, the baseline distortion at the beginning of the normal signal needs to be removed. The identification of the saturation region is based on finding very low local root-mean-squared (RMS) values within 20 time ticks. The removal of the baseline distortion is based on the so-called "adaptive baseline" technique. The right panel of Fig. 8 shows the waveform after applying the noise filter and removing the baseline distortion.

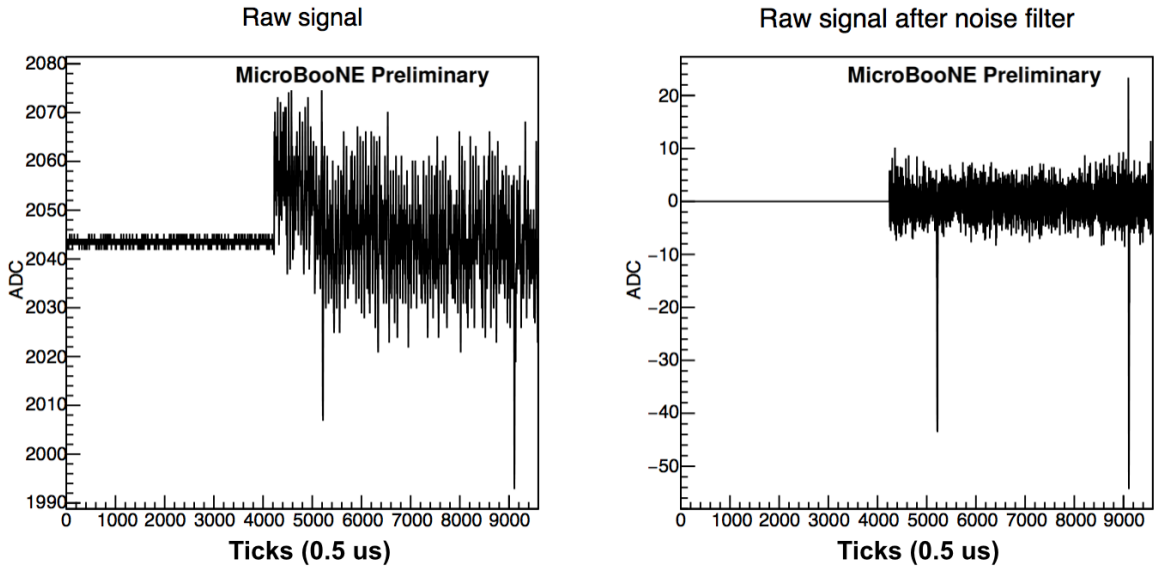

FIG. 8. An example U-plane raw waveform after the recovery of an ASIC from saturation (left). The same waveform after the noise filter (right). The region corresponding to the ASIC saturation (low RMS region) is identified. The distortion of the baseline after the ASIC saturation is removed. The DC baseline is moved to 0 after the noise filtration (right).

The saturation dependence on the wire bias points to wire motion as the most likely cause. No evidence points to any other cause. The calculation shows that a wire motion comparable to the wire diameter would induce a current sufficient to cause saturation in the presence of the electric field created by the wire bias. This is consistent with a microphonic effect. The wires are damped by the liquid so that resonant excitation by a sonic wave would be greatly reduced. A more likely cause is convective liquid motion. Saturation is less likely on shorter wires. Two steps are being planned for the next generation of large TPCs, shorter unsupported wire lengths and a choice of higher bias currents in the next version of ASICs.

2.5. Dead and High Noise Channels - Touching Wires

During the detector commissioning period, two of the V-plane wires were suspected to be loose. While a visual inspection inside the TPC did not reveal any evidence for loose wires [22], the data suggests that one of the V-planes could be connected in some way to a set of U-plane wires and the other a set of Y-plane wires. These connected wires affected many ASICs leading to either dead channels with no signals or channels with very high noise. These channels are basically unusable, and are identified by evaluating the RMS of the raw ADC signal.

A complete study of bad channels in MicroBooNE was conducted using pulser data to identify live channels and noise data to identify bad channels and noisy channels. The pedestal ADC sample distribution is used

# bad channels	Reason
96	Six ASICS on MB 24 not connected to wires
432	27 ASICs with all channels dead
334	Very noisy U wires on MBs 29-36

TABLE 1. Summary of bad channels for Run 3455 Event 6 in MicroBooNE data. A total of $\sim$ 862 channels are considered unusable. There are small variations in the number of unresponsive channels from run to run basis.

to identify bad channels as follows:

- The mean of the pedestal ADC distribution is compared to the average for the respective plane and outliers identified as bad.
- Noisy channels are identified by a pedestal RMS above a suitably high threshold.
- The FFT magnitude of the digitized waveform is integrated and used to determine if channels are bad or not connected to a wire.

A summary of dead, noise and misconfigured channels found is shown in Table 1. A set of 384 channels have a different configuration from nominal of which 352 are alive. These are not considered bad channels, but require an extra step when deconvolving the raw signal. 6 ASICs are not connected to TPC wires due to an installation error, and an additional 27 ASICs are not functioning correctly. In total there are about 433 dead channels on the U plane, 98 on the V plane and 331 on the Y plane for a total of 862 dead channels.

2.6. Low Frequency Noise from the Voltage Regulator

The last excess electronic noise to be dealt with is a low-frequency coherent electronic noise, which affects groups of channels simultaneously. This noise is typically found to be correlated across 192 channels on the same service board that contains the low voltage regulators for the front-end ASICS. Usually, the correlation is highest within the 48 channels covering 3 ASICs.

To subtract the regulator coherent noise, at each time tick, the median value of the 48 channels is calculated and is used to form a waveform to be subtracted from each of the 48 channels. This waveform is then examined to search for real signals above the noise. Before calculating the median value and subtraction, the region corresponding to the signal is identified using threshold cut based on ADC root mean square value and any region above 4 sigma is removed. But instead of making it completely 0, linear interpolation is used to connect before and after signal region. It was also noticed that the edge wires on the service board usually experience a larger contribution from the coherent noise. In order to further reduce the noise level for these edge wires, we perform a scaling adjustment according to the correlation coefficient between the median waveform to be subtracted from the channel waveform and the channel waveform itself. The scaling factor is calculated to be the ratio of the correlation coefficient and the average correlation coefficient of the 48 channels.

The waveform before and after the entire noise filter is shown in Fig. 7(top left and bottom right). The noise level is reduced by a factor of 4–5 for the induction planes and a factor of 2–3 for the collection plane. Also performance of noise filtering is shown in 2D event display in Fig. 9, 10, 11. The impact of the noise filter on signal will be discussed in Sec. 3.

On April 5, 2016, a service board serving one set of channels on feed-through 5 was modified with an additional filter circuit to remove the low frequency coherent noise. The FFT of data taken before and after the LV filter was added is shown in Fig. 12. A significant reduction in the low frequency component of the noise was observed that is consistent with the level of reduction in noise observed after the software coherent noise filter.

3. IMPACT OF NOISE FILTERING ON SIGNAL

In this section, we will study if noise filtration process has any effect on the real signal. As seen from the previous sections in Figs. 7 and 8, the software filter in general has negligible impact on the real signal. The only operation that would lead to distortion of the waveform is the regulator noise removal discussed

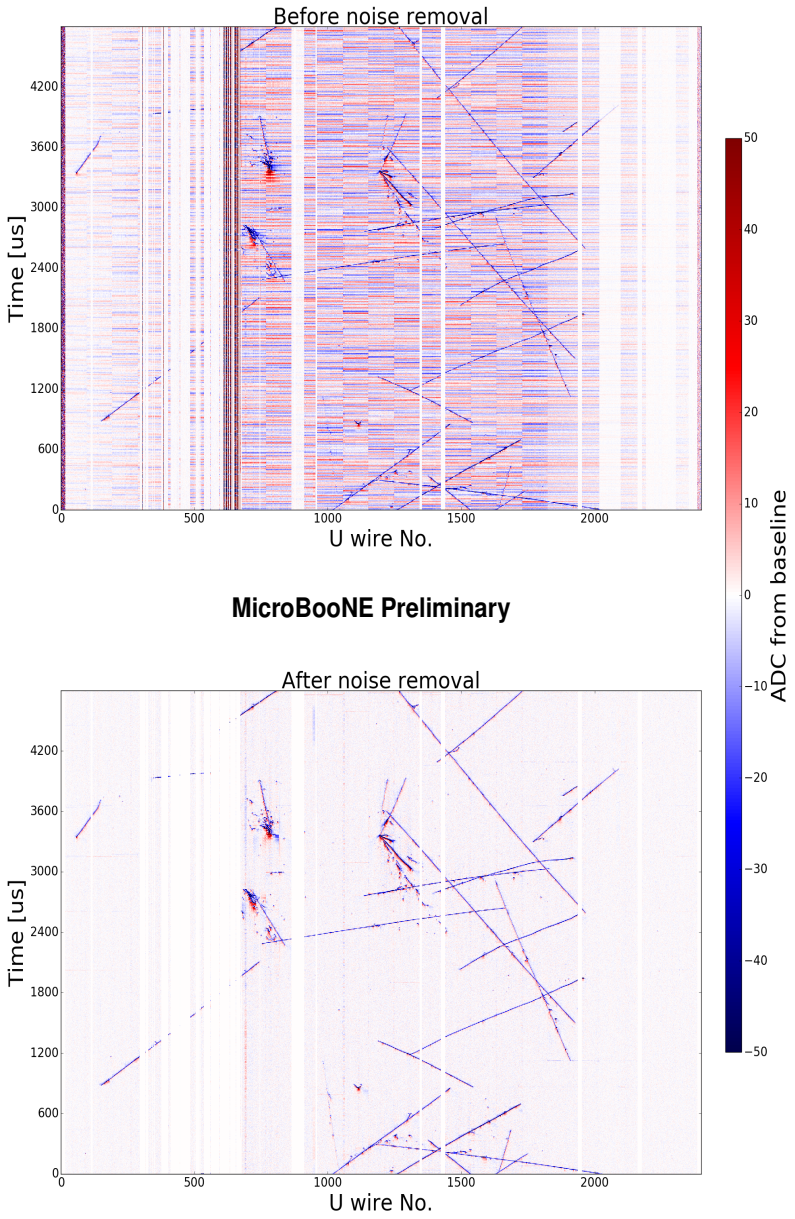

FIG. 9. 2D event display of U-plane from Run 3493 Event 41075 showing raw signal before and after noise filtering.

in Sec. 2.6. This is particularly true for charged particle tracks traveling parallel to the wire plane. In this case, the ionized electrons would reach all the wires (out of the 48 channels used in the subtraction) at the same time and the default coherent noise removal procedure can remove the signal - which is coherent across many adjacent wires - as well as the noise. Special protection is added to avoid removing real signals, but the effectiveness of this protection decreases the closer the signal size is to the coherent noise.

In order to examine the performance of the coherent noise filter on the data, a simulated data study overlays pulse shapes on top of recorded TPC data. The pulse shapes correspond to the impulse response of the FE electronics for a given input charge to the front end amplifiers. Pulse shapes are overlayed on either one channel per group of correlated channels or on all channels simultaneously as shown in Fig. 13. This figure shows an example waveform before any noise noise filtering is applied, where the small regularly

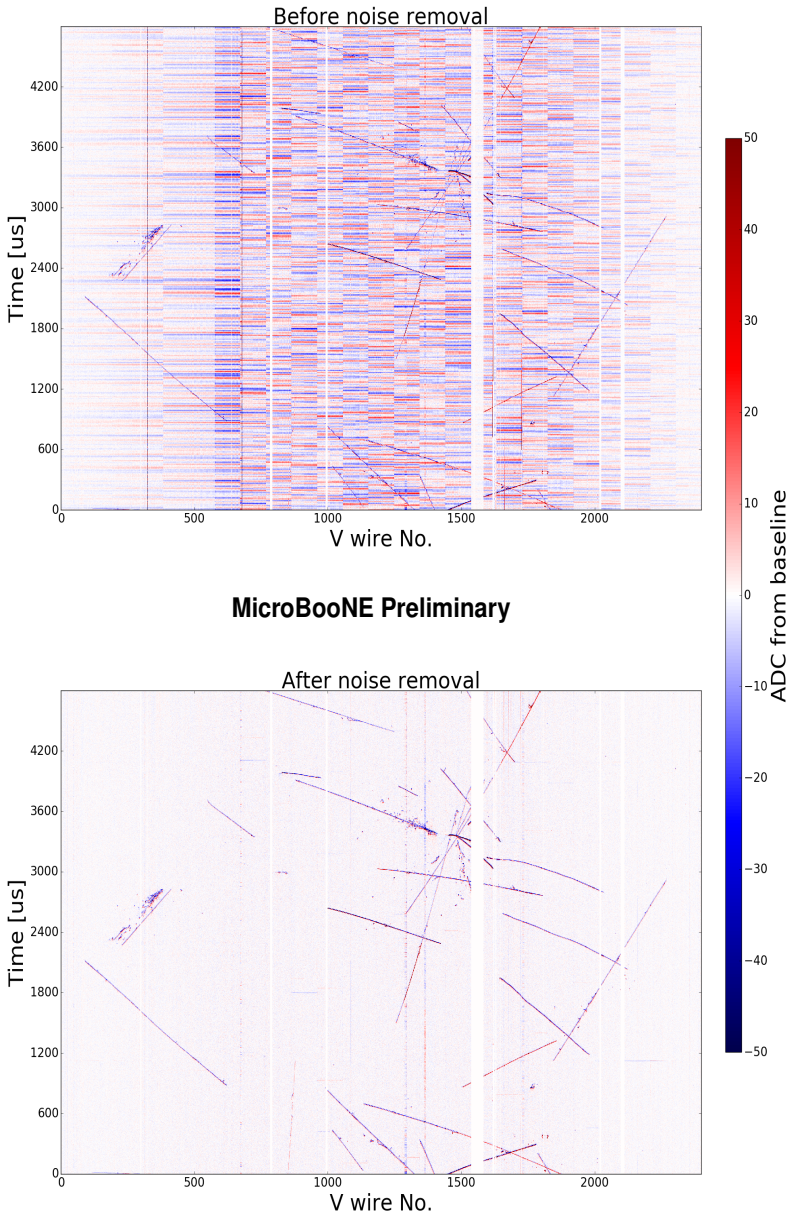

FIG. 10. 2D event display of V-plane from Run 3493 Event 41075 showing raw signal before and after noise filtering.

spaced pulses ∼50ADC counts high are the simulated pulse shapes. The large pulse corresponds to an actual cosmic pulse found in the real data.

Overlaying pulse shapes on all channels simultaneously corresponds to the time distribution of ionization signals that are most likely to be removed by coherent noise removal and is the focus of this test. Simulated electronics impulse response signal shapes with sizes between 1000 e- to 20000 e- on the front-end amplifier inputs are overlayed on every channel simultaneously, and the resulting waveforms processed by the noise filtering process. The impact of the filtering process on electronics signals is evaluated by measuring the resulting pulse height and comparing them to the expected values. The bias in measured pulse height as a function of simulated signal size summarized in Fig. 14 shows that small signals are suppressed by the noise filtering process when signals are overlayed simultaneously on all three planes. This suppression largely

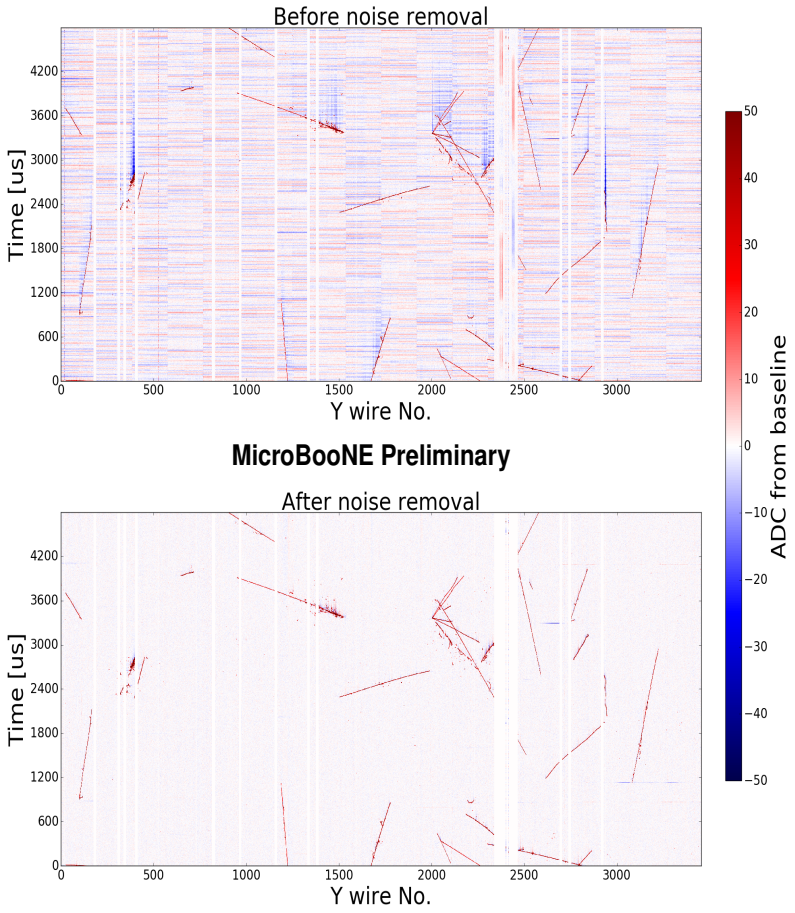

FIG. 11. 2D event display of Y-plane from Run 3493 Event 41075 showing raw signal before and after noise filtering.

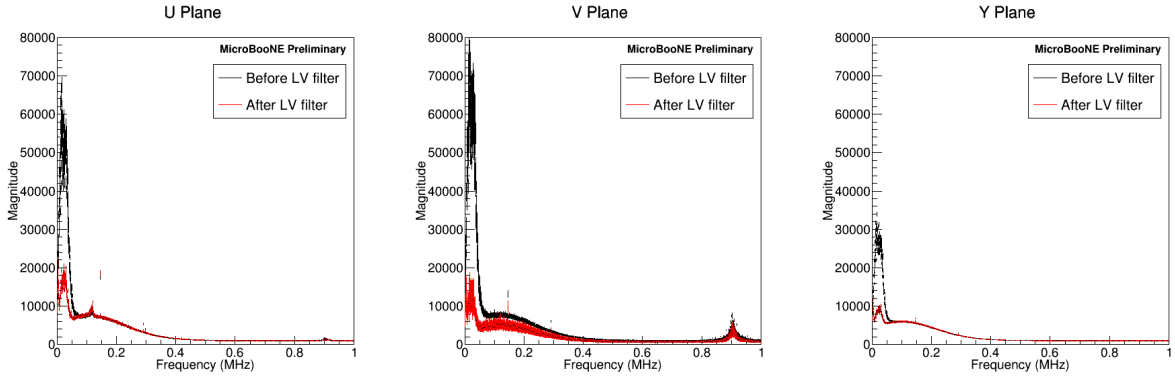

FIG. 12. The FFT of the data on the U (left), V(center) and Y (right) planes before (black color) and after (red color) the hardware filter was added to the low-voltage service board on feedthrough 5.

disappears for impulse response signals greater than 5000 e-, corresponding to pulse heights of ∼30 ADC counts. Signals of this size are large enough so that they are not included in the "median waveform" that is subtracted from all channels. As a result, they are not removed by the coherent noise filter.

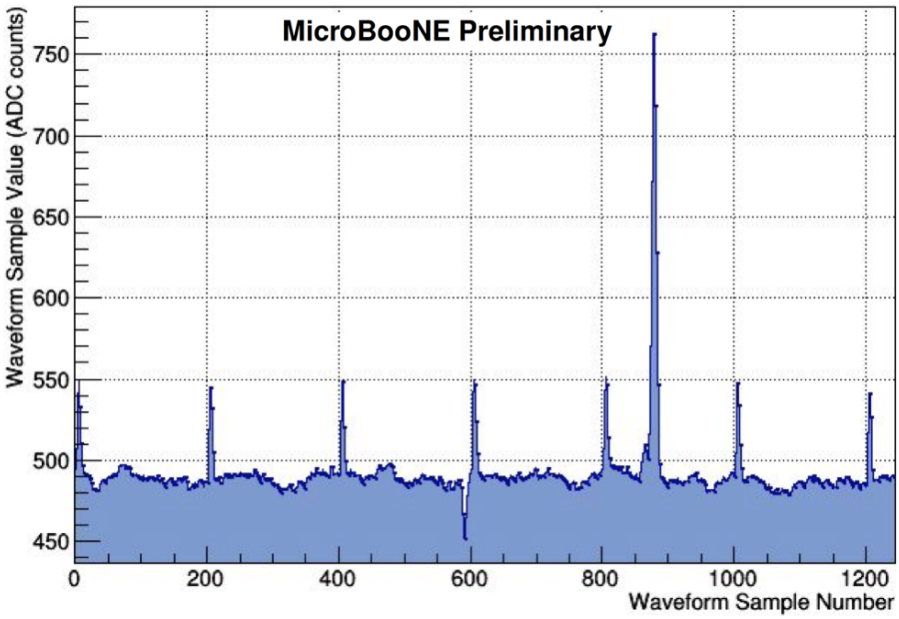

FIG. 13. Simulated pulse shapes in single channel corresponding to the impulse response of the FE electronics overlaid on real data with a cosmic signal before any noise filtering. The large pulse around 900 Sample Number corresponds to an actual cosmic pulse found in the real data.

4. RESIDUAL NOISE LEVELS

Fig. 15 shows the calculated electronic noise in terms of the ADC RMS value after all noise filtering is performed. The ADC RMS value at each stage of the software noise filtering. There are ∼860 channels not shown in these plots that were identified as either dead, disconnected or unusable due to very high noise as described in Sec. 2.5 and were therefore not considered for noise removal.

The remaining channels with high ADC RMS are each examined carefully in both the time and frequency domain. Although the observed noise spectra on these channels are quite different from the majority of the "good" channels, good signals can still be seen. Therefore, we keep these channels for further analysis. Fig. 16 shows the calculated electronic noise in terms of the ADC RMS value after removing these high RMS channels (∼84 channels in run 3455). The time-dependance of noise will be studied in detail in near future.

Fig. 17 illustrates the dependence of the electronic noise magnitude on the wire length, L. A linear fit was made to the noise level as a function of wire length:

$$\text{Noise}_{\text{RMS}}\ (ADC) = 1.019 + 0.00173 \times L(cm). \tag{5}$$

The noise level in terms of ADC can be converted to the equivalent noise charge (ENC) as follows:

$$1\ \text{ADC} = 1\ \text{ADC} \times \frac{2000\ mV}{4096\ \text{ADC}} \times \frac{1\ fC}{14\ mV} \times \frac{1}{1.1} \times \frac{6241\ \text{electrons}}{fC} = 198\ \text{electrons}. \tag{6}$$

Here the factors of 14 mV/fC and 1.1 are the gain of the cold ASIC and the intermediate amplifier, respectively. Therefore, the nominal ENC for the induction wires is about 400 electrons, which is the lowest of LArTPC's greater than 100 tons to date, past or present.

From Eq. 5 and Eq. 6, the expected ENC on a wire of 12 m - which corresponds to an input capacitance of 220 pF - with a 2 μs shaping time would be 610 electrons, which is in excellent agreement with the test-stand measurements at BNL of the ASIC in the cold as shown in Fig. 5.

A parameterization of the electronic noise level using Eq. 5 can be implemented in simulation.

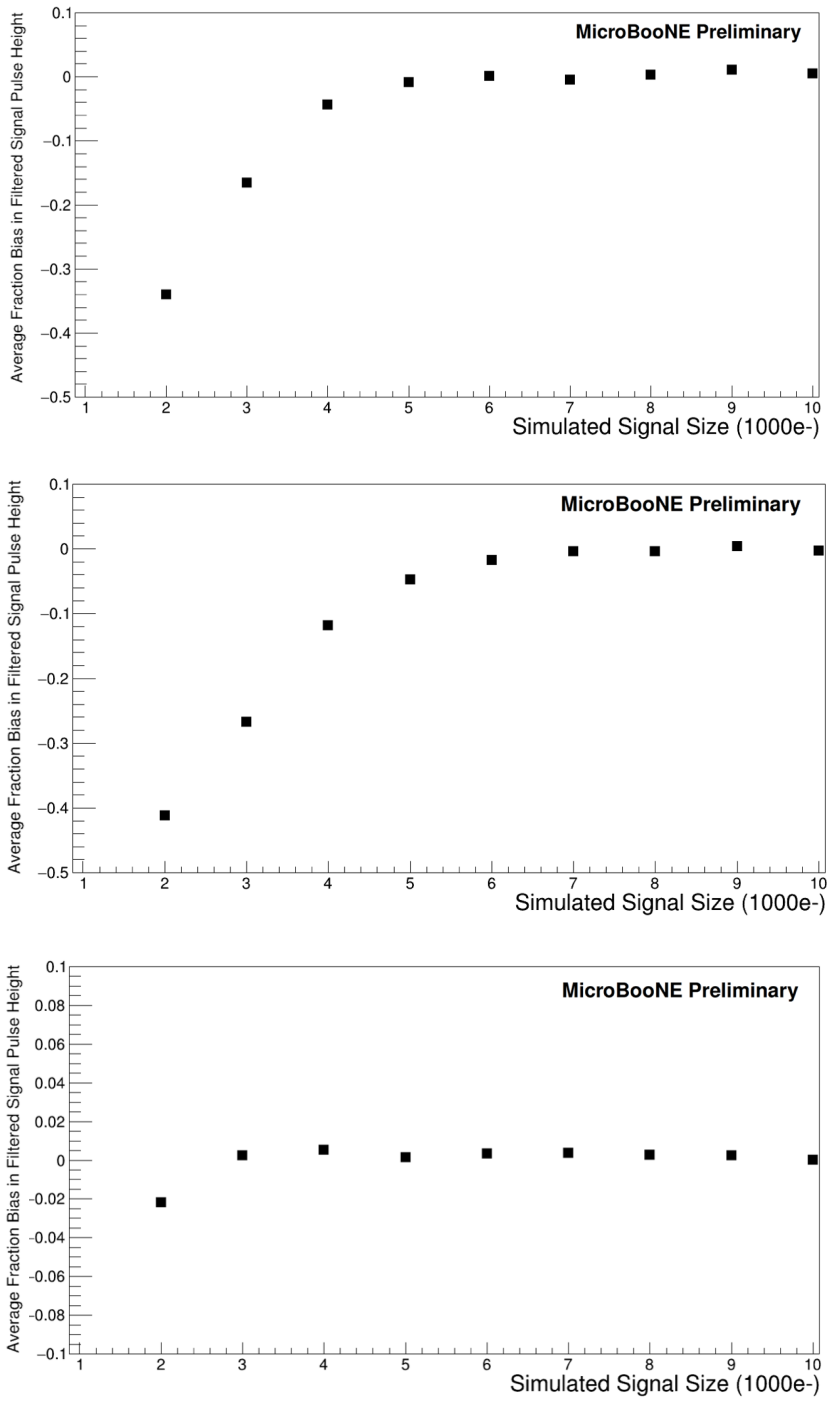

FIG. 14. Examination of the software noise filter impact on signals. The case shown here is the worst case scenario or affects a small number of tracks. Impulse response signals of various sizes are overlayed on all channels simultaneously before applying the noise filtering process. U-plane (top panel), V-plane (middle panel) and Y-plane (bottom panel). The suppression in signal size due to the filtering process becomes very small for signals greater than 5000 e-. Note that dead channels are identified as described in Sec. 2.5 and not included in this bias measurement.

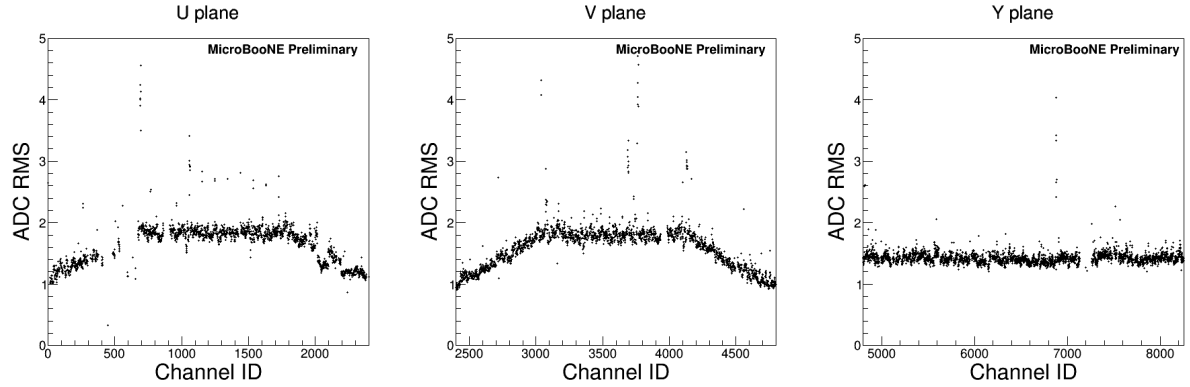

FIG. 15. The residual noise level after filtering in terms of the RMS value for all channels (except dead channels) from Run 3455 Event 6 is shown for U, V, and Y planes.

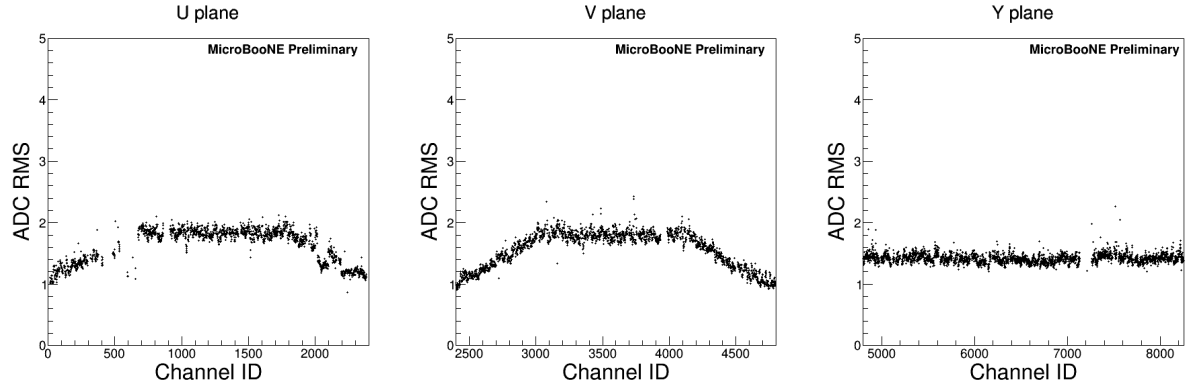

FIG. 16. The residual noise level after filtering in terms of the RMS value vs. channel number after removing dead channels and known bad channels from Run 3455 Event 6.

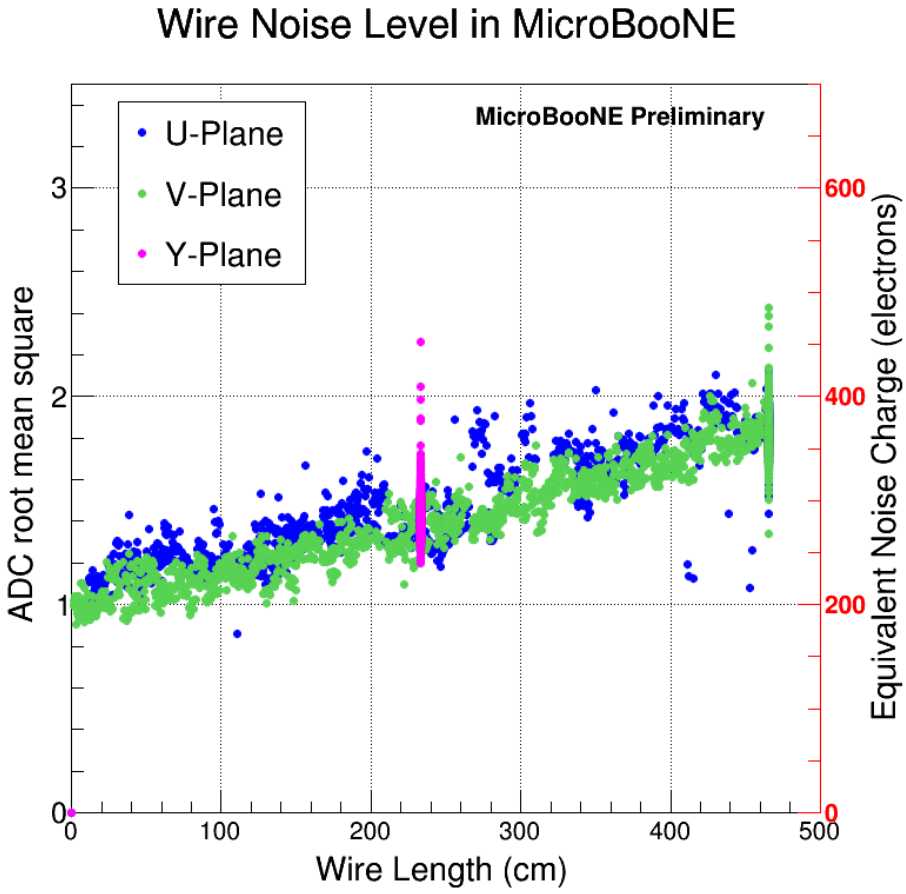

FIG. 17. The noise level in terms of the RMS value and ENC is plotted with respect to the wire length. The vertical band in magenta are all of the Y-plane wires which have the same length and the vertical green band at the right most end of the plot is all longest wires from U and V-planes.

5. PEAK SIGNAL-TO-NOISE RATIO

In a LArTPC, the signal-to-noise ratio (S/N) is often used as a convenient metric to describe the performance of the detector. However, a clear and common definition of S/N needs to be established before one can compare this metric among different detectors. While the level of noise can be clearly described by the *Equivalent Noise Charge* (ENC), both before and after software noise filtering, the level of signal depends on many factors such as the event topology of the initial energetic particle, LAr properties, TPC field response and TPC wire spacing. Therefore it needs to be carefully defined.

A simple "standard candle signal" for *collection wires* is a MIP muon traveling parallel to the wire planes and perpendicular to the collection wires. This muon is expected to produce $\sim$ 9000 electrons per mm, which reduces to $\sim 6000\,e^-$ per mm after recombination. With the 3 mm wire spacing at MicroBooNE, the collection plane is expected to collect $\sim 18000\,e^-$ per wire for this muon. Since the Equivalent Noise Charge is about 400 electrons after noise filtering as shown in Fig. 17, the S/N for collection wires could be as high as $\sim 60:1$. Similar metrics can be defined for *induction wires* by selecting MIP muons with different orientation, or correcting for the path length. Such numbers can then be compared among different experiments with the understanding that the differences in the wire length (for noise) and wire pitch (for signal) among detectors will contribute to the differences in S/N.

While such a metric is simple and clear, it assumes that the true signals can be extracted from the raw waveforms, which often requires the procedure of deconvolution to remove the effect of the field response. While such a procedure is relatively straightforward for collection wires, it is rather complicated for induction wires due to the bi-polar nature of their signal shapes. Details of the techniques to extract the true signals via deconvolution can be found in Ref. [23]. To avoid a more complicated analysis, an even simpler metric can be defined which uses only the raw unprocessed waveforms. One such metric that we define in this note is the *Peak Signal to Noise RMS* (PSNR), where the peak signal is the peak of the absolute ADC value in a signal region, and noise RMS is the root-mean-square ADC value in the pedestal region. It is useful to look at this metric both before and after software noise filtering is done; the former establishes the baseline significance at which we can extract signals from noise, while the latter demonstrates our maximal reach. We note several important points concerning the limitations of this metric :

- The size of the peak signal is expected to be different between collection wires and induction wires. This is mainly due to the bi-polar nature of the induction wires, causing the induction peak signal to be smaller. However, in induction signals, the negative region contains equal information as the positive region. Therefore, the true signal after proper deconvolution is still the same as the collection wires.

- The size of the peak signal is expected to be different between the U and V induction wires because of the different field response between the two and also depends on wire bias settings. As a reference, from both the data and Garfield 2D simulation (Fig. 10 of Ref. [23]), the peak signal for a point charge compared to the collection plane is about a half for the U plane and a third for the V plane in MicroBooNE.

- The size of the peak signal on the induction wires is strongly dependent on the event topology of the charged particle trajectories. For large-angle tracks with respect to the wire plane, for example, the *dynamically-induced charge effect* (charge induced on further-away wires) can cause significant cancellation of the induction signal, leading to a very small peak signal in the raw waveform. The true signal can only be extracted after proper deconvolution.

- Since induction wires have variable lengths, the noise RMS is different for different induction wires.

With these caveats in mind, in Fig. 18 the PSNR is plotted for all three planes both before and after software noise filtering, showing results from ten different events as an example. Data events triggered with external triggers (from a pulser) were used, providing a sample of cosmic events with which to estimate the peak signal-to-noise ratio. We should note that not only MIPs (e.g. cosmic muons) are included in this sample, but also other cosmogenic particles, as well as other activity in the TPC, such as the decay of radioisotopes (such as Ar-39). Any particle within the TPC leading to ionization is included as signal, as long as the significance of the signal peak is reasonably high with respect to the noise RMS (greater than 4-sigma).

Looking at Fig. 18, besides the known difference among the three planes as we emphasized previously, we notice that the PSNR increases dramatically after software noise filtering by roughly a factor of two for all

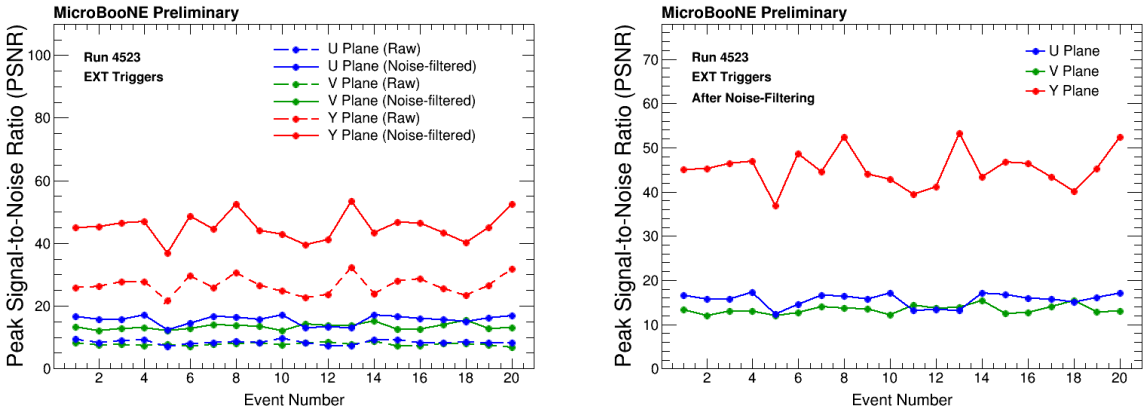

FIG. 18. Peak signal-to-noise ratio for all three planes both before ("Raw") and after ("Noise-filtered") software noise filtering. Results from ten events in data taken with external triggers are shown (left). Zoomed in peak signal-to-noise ratio for all three planes after software noise filtering (right).

three planes. The estimated PSNR for each plane, before and after software noise filtering, are summarized in Table 2.

Waveform Type	**U Plane PSNR**	**V Plane PSNR**	**Y Plane PSNR**
Raw	8.6	7.7	26.7
Noise-filtered	15.8	12.9	45.3

TABLE 2. Summary of peak signal-to-noise ratio for each plane, both before and after software noise filtering. PSNR increases by roughly a factor of two for all three planes after software noise filtering.

6. SUMMARY AND CONCLUSION

In this technote, the different characteristics of the MicroBooNE TPC noise in excess of the expected front-end ASIC noise are presented. The noise is characterized in both the frequency and time domain, as well as by wire and channel number. A discussion of possible sources of the excess noise are also presented. A software filter to eliminate most of the excess noise is implemented and the performance of the filter and its impact on the signal was discussed. Table 3 summarizes the characteristics of the observed excess TPC noise signals in MicroBooNE:

TABLE 3. Summary of the observed TPC noise in MicroBooNE. The estimated contribution to the total ENC for the longest wires in each plane is presented in the 4th column.

Noise	Frequency range	Plane Impacted [a]	ENC in e- (Plane)	Possible Source
Burst	$\sim$ 900 kHz	U , V, Y	negligible [b] at 2 μs shaping time	Field pick-up on wires (?)
Single frequency	$\sim$ 36 kHz	U , V	920 (U), 380 (V), 0 (Y)	HV Supply
Single frequency	$\sim$ 108 kHz	U	750 (U), 0 (V), 0 (Y)	HV Supply
ASIC saturation	$<$ 20 Hz	U, V, Y	unknown [c]	Wire motion (?)
Regulator	$<$ 50 kHz	U, V, Y	1030 (U), 1300 (V), 550 (Y)	LV regulators
Cold ASIC			430(U), 420 (V), 330 (Y)	Design spec
Total			1600 (U), 1400 (V), 660 (Y)	

[a] Bad channels identified in Sec. 2.5 are excluded from noise studies.

[b] As described in Sec. 2.2, this noise is largely suppressed after choosing 2μs shaping time. The bursts of this noise are intermittent (non-stationary) with amplitude varying in time

[c] It is hard to quantify ENC associated with ASIC saturation without studying effect of microphonics in details which is beyond the scope of this document.

The noise level (ENC) after the noise filtering is in general below or about 400 electrons for 85% of MicroBooNE channels. There are ∼100 high-noise channels. The achieved ENC is consistent with the expected performance of the cold electronics [16] and represents the best currently achieved in LArTPC's greater than 100 tons.

In addition to the characterization of the excess noise in the MicroBooNE TPC, high noise channels that are unusable and dead channels have been identified through studies of the noise and pulser data. There are about 10% channels that are unusable for the physics analysis. The impact of these unusable channels depends on the reconstruction strategy. By requiring two wire planes instead of three wire planes, the inefficiency is estimated to be about $1-(0.9^3+3\times0.9^2\times0.1)\sim3\%$. Also, the measured efficiency requiring two wire planes using implemented algorithm [24] with real location of dead channels is about 97.3%, which is consistent with the estimation. More dedicated studies will be carried out in the future. Table 1 summarizes the number and causes of dead channels in MicroBooNE.

Finally, we note that the two excess noise sources which impact the largest number of channels (and events), the HV power supply noise and the LV regulator noise are in the process of being removed by hardware means. These hardware upgrades will make the corresponding steps in software filter unnecessary, which would completely eliminate the distortion in signal due to software filtering.

[1] C. Rubbia, "The Liquid Argon Time Projection Chamber: A New Concept for Neutrino Detectors," CERN-EP-INT-77-08.

[2] W. Willis and V. Radeka, Nuclear Instruments and Methods **120**, no. 2, 221-236 (1974).

[3] H. H. Chen, P. E. Condon, B. C. Barish, and F. J. Sciulli. A Neutrino detector sensitive to rare processes I. A Study of neutrino electron reactions. FERMILAB-PROPOSAL-0496, 1976.

[4] S52 D. R. Nygren. The Time Projection Chamber: A New 4 pi Detector for Charged Particles. eConf. C740805:58 (1974).

[5] H. Chen et al., "Proposal for a New Experiment Using the Booster and NuMI Neutrino Beamlines: MicroBooNE," 2007. FERMILAB-PROPOSAL-0974.

[6] MicroBooNE Technical Design Report, `http://www-microboone.fnal.gov/publications/TDRCD3.pdf`

[7] J. Conrad et al., "The Photomultiplier Tube Calibration System of the MicroBooNE Experiment," JINST **10**, T06001 (2015).

[8] V. Radeka et. al., "Cold Electronics for 'Giant' Liquid Argon Time Projection Chambers," J. Phys. Conf. Ser. **308** (2011) 012021.

[9] Y. Li et al. Nucl. Inst. Meth. A816, 160 (2016). `http://lar.bnl.gov/properties/`

[10] The MicroBooNE Collaboration, "Measurement of Average Drift Velocity Utilizing UV Laser Data", MicroBooNE-Note-1009-Pub.

[11] The MicroBooNE Collaboration, "Noise Dependence on Temperature and LAr Fill Level in the uBooNE Time Projection Chamber", MicroBooNE-Note-1001-Pub.

[12] Inverse Laplace Transform, `https://en.wikipedia.org/wiki/Inverse_Laplace_transform`

[13] A resistor-capacitor (RC) circuit is an electric circuit composed of resistors and capacitors driven by a voltage or current source and can be used to filter a signal by blocking certain frequencies and passing others.

[14] Deconvolution, `https://en.wikipedia.org/wiki/Deconvolution`

[15] V. Radeka, "Low-Noise techniques in Detectors", Ann. Rev. nucl. Part. Sci. 38 (1988) 217.

[16] De Geronimo, Gianluigi et al., "Front-end ASIC for a Liquid Argon TPC", IEEE Trans.Nucl.Sci. 58 (2011) 1376-1385.

[17] Known colloquially by the collaboration as "Zig-Zag noise".

[18] The convolution of the mis-configured channels with a 2μs response function effectively filters out this noise as well.

[19] Initially dubbed "chirping".

[20] The LAr FE ASIC, bias current is programmable as 100 pA or 500 pA. The default 500 pA gives 60 electrons noise.

[21] An event is one DAQ time frame of 4.8 ms.

[22] B. Carls et. al., "Design and operation of a setup with a camera and adjustable mirror to inspect the sense-wire planes of the Time Projection Chamber inside the MicroBooNE cryostat", arXiv:1507.02508.

[23] M. Bishai et. al. "A Method to Extract the Charge Distribution Arriving at the TPC Wire Planes in MicroBooNE", MicroBooNE-Note-1017-Pub.

[24] `https://github.com/BNLIF/wire-cell`